J Mater Sci (2008) 43:5185–5192
DOI 10.1007/s10853-008-2741-8

Tungsten carbide nanopowder by plasma-assisted chemical vapor synthesis from WCl_6–CH_4–H_2 mixtures

Taegong Ryu · H. Y. Sohn · Kyu Sup Hwang · Zhigang Z. Fang

Received: 23 January 2008 / Accepted: 16 May 2008 / Published online: 3 June 2008

Abstract Nanosized tungsten carbide powder was prepared by a thermal plasma process using tungsten hexachloride (WCl_6) as the precursor. The reduction and carburization of the vaporized precursor by methane–hydrogen mixtures produced nanosized WC_{1-x} powder, which sometimes contained WC and/or W_2C phase. The effects of the molar ratio of reactant gases, plasma torch power, the flow rate of plasma gas, and the addition of secondary plasma gas (H_2) on the product composition and grain size were investigated. The tungsten carbide powder produced by the plasma process showed particle sizes less than 20 nm. The produced powder was heated in hydrogen to fully carburize the WC_{1-x}, and W_2C phases to the WC phase as well as to remove excess carbon in the product. Finally, WC powder with particle size less than 100 nm was obtained.

Introduction

Among the hard alloys and refractory carbides, tungsten carbide has come a long way since its introduction in the early 20th century. Due to the much-desired properties of high hardness and good wear resistance, tungsten carbide has many industrial applications. It is applied to tools in the metalworking and drilling and mining industries under high pressure, high temperature, and corrosive environments. Mechanical properties such as hardness, compressive strength, and transverse rupture depend on the composition and microstructural parameters such as the grain size of WC [1–4]. Previous investigations [5–11] also have shown that the reduction of tungsten carbide grain size gives a significant improvement of the mechanical properties. Thus, the production of nanosized tungsten carbide powder is critical.

Nanosized powders have been produced by various methods such as the thermo-chemical spray drying process [12–13], mechanical alloying (MA) [14–16], and chemical vapor condensation (CVC) [17]. Recently, an innovative plasma processing technique has been developed for the chemical vapor synthesis (CVS) of nanosized powders [18–21]. CVS is a process for making fine solid particles by the vapor-phase chemical reactions of precursors. The thermal plasma process provides a high processing rate as well as other advantages for the synthesis of nanosized powder such as high processing temperature up to about 10,000 K to allow the use of a wide range of reactants, clean reaction atmosphere which is required to process high-purity products, and a high quenching rate to form ultrafine powders. Many articles on the thermal plasma synthesis of metals, ceramics, and composites in recent years have reported on the advantages of thermal plasma as one of the most promising methods for the industrial production of nanosized powders [22–24].

For the preparation of fine tungsten carbide powder, compounds such as tungsten hexachloride (WCl_6) [25], tungsten hexafluoride (WF_6) [26], and tungsten hexacarbonyl ($W(CO)_6$) [27] are generally favored as precursors based on their relatively low evaporating temperatures as well as the ease of reduction by hydrogen. Several carburizing agents such as propane (C_3H_8) [28], acetylene (C_2H_2) [29], and methane (CH_4) [30–32] have also been used. Methane is the most commonly used carburizing

T. Ryu · H. Y. Sohn (✉) · K. S. Hwang · Z. Z. Fang
Department of Metallurgical Engineering, University of Utah, Salt Lake City, UT 84112, USA
e-mail: h.y.sohn@utah.edu

agent because it is most readily available and stable up to a high temperature [33].

In this work, nanosized tungsten carbide powder was synthesized by a thermal plasma process using WCl_6 as the precursor. Various processing parameters were emphasized to optimize the process for the production of nanosized tungsten carbide powder. The effects of experimental variables such as the molar ratio of reactant gases, plasma torch power, the flow rate of plasma gas, and the addition of the secondary plasma gas (H_2) were investigated. The produced powder, which consisted mainly of WC_{1-x} phase, was subjected to heat treatment under hydrogen and the resulting product was analyzed for composition, grain size, and carbon content.

Experimental

Plasma reactor system was equipped with a plasma generator with a downward plasma torch, a power supply unit, a cylindrical reactor, a cooling chamber, a cooling system, a precursor feeding system, a powder collector, a gas delivery system, an offgas scrubber containing 5% NaOH solution, and an offgas exhaust system, as shown in Fig. 1. The plasma torch consisted of a water-cooled tungsten cathode and a copper anode nozzle operating at atmospheric pressure. The reactor consisted of a vertical water-cooled stainless-steel tube of 15 cm inner diameter and 60 cm length and an inner graphite cylinder of 7.6 cm inner diameter and 60 cm length. Graphite felt was placed between the graphite tube and the inner wall of the water-cooled stainless-steel tube for the insulation of the reactor. The cooling chamber connected to the bottom of the reactor was a water-cooled two-layer stainless-steel box to cool the outgoing gas to a temperature lower than 150 °C. A data acquisition system recorded the temperatures of the reactor exit gas, the input and output cooling water, and outgoing gas from the cooling chamber. The precursor feeding system consisted of an entrained-flow powder feeder, a vibrator, a carrier gas line, a sample container, and a water-cooled delivery line through which the precursor was fed toward the outside boundary of the visible plasma flame (7 mm diameter) from a distance of 15 mm near the exit of the plasma torch. Argon (99.9%) and hydrogen (99.9%) were used as the primary and the secondary plasma gas, respectively. Argon, used as the primary plasma gas, was also separately passed through the powder feeder as the carrier gas as well as an inert gas to keep the atmosphere in the container inert. Before delivering the precursor into the plasma flame, the reactor was heated by the plasma flame generated until its temperature reached a steady level.

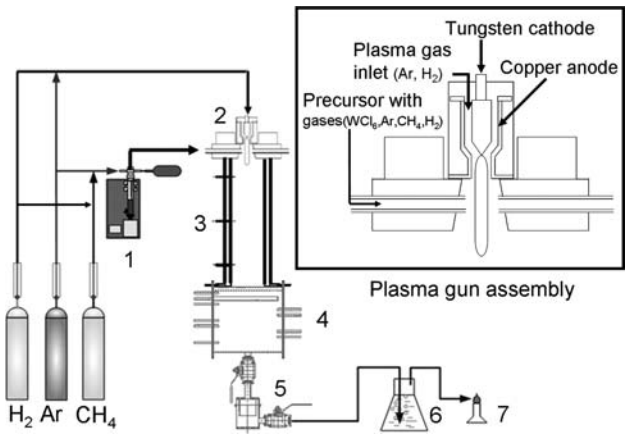

Fig. 1 Schematic diagram of the plasma reactor system: (1) entrained-flow powder feeder of WCl_6, (2) plasma gun, (3) cylindrical reactor, (4) cooling chamber, (5) powder collector, (6) scrubber, and (7) Bunsen burner

Tungsten hexachloride of 99.9% purity was used as the precursor. Hydrogen (99.9%) and methane (99.9%) were used as the reducing and carburizing agents, respectively. The produced powder was collected using a Teflon-coated polyester filter with a pore size of 1 μm. The reactor was purged with an Ar flow of 5 L/min (25 °C, 86.1 kPa total pressure at Salt Lake City) for 10 min before and after each experiment. The detailed experimental conditions are discussed in the Results and Discussion section since these results were based on various experimental conditions. The product was analyzed by the use of XRD (Siemens D 5000) and the morphology with particle size analysis was done by the use of TEM (JEOL, JEM-3000F). The total carbon content of the powders was measured with a Carbon Determinator (LECO CS-444). The grain size of the synthesized powders was calculated from the XRD pattern by applying the Scherrer equation [34].

Results and discussion

Preliminary experiments

Initial experiments were conducted to find optimum conditions at which tungsten carbide could be produced in WCl_6–H_2–CH_4 system. The experimental conditions are as follows; the feeding rate of WCl_6 was 3.5 g/min, the flow rate of Ar–H_2–CH_4 mixture to carry the WCl_6 powder was 4 L/min (25 °C, 86.1 kPa), the applied plasma torch power was 13 kW, and the flow rate of primary plasma gas (Ar) to generate plasma flame was controlled at 38 L/min (25 °C, 86.1 kPa) in which no secondary plasma gas (H_2) was used.

The main product under these conditions was WC_{1-x} with small amounts of W_2C and WC phases, as shown in Fig. 2. This result is consistent with the phase diagram available in the literature [35], which indicates that WC_{1-x} is likely the first stable solid tungsten carbide phase formed as the W-C liquid solution cools toward solidification at 2,710 °C. After the initial formation the WC_{1-x} phase may be carburized to WC. Further, this phase decomposes into WC and W_2C phases below 2,530 °C. However, the rapid quenching of the produced particles, which provides little time for either decomposition or further carburization, resulted in the WC_{1-x} phase remaining as the major phase in the collected product. Figure 2 also shows the XRD patterns of the products obtained with different CH_4/H_2 ratio in the feed stream. Crystalline phases were identified by comparing the experimental data with the Joint Committee of Powder Diffraction Standards (JCPDS) files from the International Center for Diffraction Data. The amount of W_2C and WC decreased as the CH_4/H_2 ratio was increased and when CH_4 alone was used as the reaction gas, the product was WC_{1-x}. The grain size of WC_{1-x}, 13 ± 1 nm, decreased to 9 ± 1 nm when no H_2 was used.

The results of these experiments indicated that methane alone was enough to reduce and carburize tungsten hexachloride to tungsten carbide. Thus, the subsequent experiments were performed without the hydrogen addition in the feed stream. Further, these and the subsequent experiments showed that the conversion of WCl_6 to tungsten carbides was complete in the plasma reactor as long as methane was added in excess of the stoichiometric amount.

The results obtained from the preliminary experiments conducted in the thermal plasma process showed a considerable promise compared with other conventional processes, owing to the high temperature generated by the plasma flame to rapidly volatilize the precursor (WCl_6) and the rapid quenching of the product to yield nanosized tungsten carbide powder.

Other factors that significantly affect the WC_{1-x} formation were further tested, as described below.

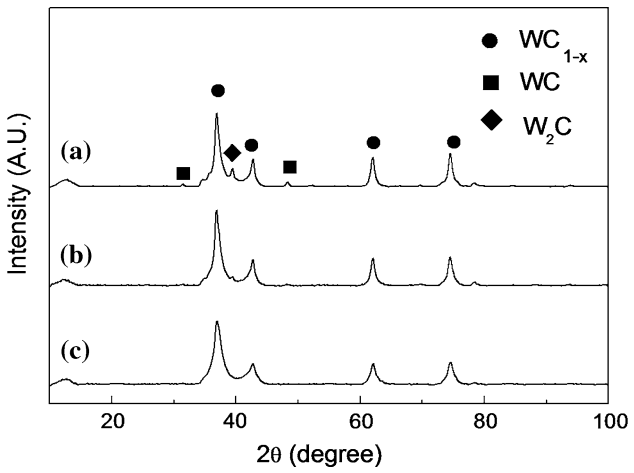

Fig. 2 X-ray diffraction patterns of the products obtained with different CH_4/H_2 ratios: (a) $[CH_4/H_2] = 0.5$, (b) $[CH_4/H_2] = 1$, and (c) only CH_4

Effect of plasma torch power

Experiments were conducted to investigate the effect of plasma torch power by varying it from 11 to 32 kW while maintaining all other conditions constant [flow rate of primary plasma gas (Ar) of 57 L/min (25 °C, 86.1 kPa) in which no secondary plasma gas (H_2) was used, WCl_6 feeding rate of 3.5 g/min, C/W ratio of 6.3, and flow rate of Ar–CH_4 mixture to carry the WCl_6 powder was 2.5 L/min (25 °C, 86.1 kPa) with no H_2]. The ratio of H_2 produced from CH_4 to H_2 required to reduce WCl_6 was 4.2 at the C/W ratio of 6.3. The pressure in the reaction chamber was always 86.1 kPa. Figure 3 shows the XRD patterns of the products obtained with different power levels of the plasma torch. The main product was WC_{1-x} and the amounts of WC and W_2C were small in all cases. The grain size of WC_{1-x} obtained at a power level of 11 kW was 8 ± 1 nm and increased to 16 ± 1 nm as the applied power was increased to 19 kW or higher, up to 32 kW. The particle size of WC_{1-x} was also examined using TEM micrographs. Figure 4 shows that the particle size of WC_{1-x} obtained at a power level of 11 kW was less than 10 nm and it increased to about 20 nm at an increased plasma torch power of 32 kW. The morphology of produced particles was mostly round. It is noted that these values are from measurements on a rather limited number of particles. The particle size obtained from the TEM micrograph was close to the grain size calculated from the XRD results. Thus, the particles produced by the plasma process seem to be single crystals and it is reasonable to use the calculated grain size from the XRD results as the particle size. Since excess methane was used in the reaction, free carbon was also present in the product.

Effect of plasma gas flow rate

Experiments were performed to determine the effect of plasma gas flow rate by varying the flow rate of the primary plasma gas (Ar) from 29 L/min (25 °C, 86.1 kPa) to 75 L/min (25 °C, 86.1 kPa) in which no secondary plasma gas (H_2) was used under otherwise identical conditions [plasma torch power of 13 kW, WCl_6 feeding rate of 3.5 g/min, C/W ratio of 6.3, and flow rate of Ar–CH_4 mixture to carry the WCl_6 powder of 2.5 L/min (25 °C, 86.1 kPa) with no H_2]. The main product was WC_{1-x} with a small amount of WC, as shown in Fig. 5. Although small in all cases, the amount of WC decreased as the plasma gas flow rate was

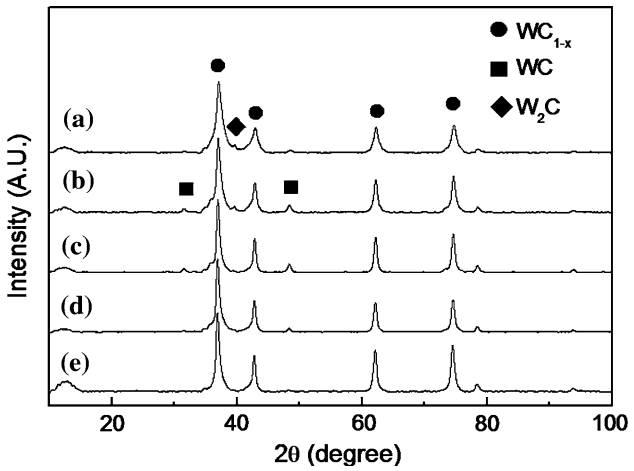

Fig. 3 X-ray diffraction patterns of the products obtained from (a) 11 kW, (b) 15 kW, (c) 19 kW, (d) 25 kW, and (e) 32 kW

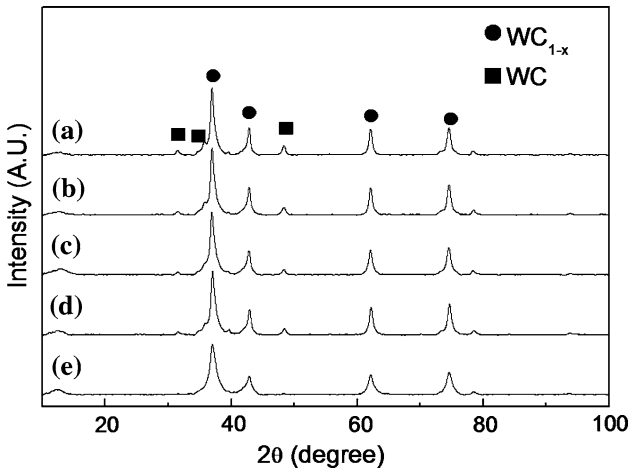

Fig. 5 X-ray diffraction patterns of the products obtained with various flow rates of primary Ar: (a) 29 L/min (25 °C, 86.1 kPa), (b) 38 L/min (25 °C, 86.1 kPa), (c) 48 L/min (25 °C, 86.1 kPa), (d) 57 L/min (25 °C, 86.1 kPa), and (e) 75 L/min (25 °C, 86.1 kPa)

increased. This reduced the time for WC_{1-x} to be further converted to WC. The grain size of WC_{1-x} obtained at the plasma gas flow rate of 29 L/min (25 °C, 86.1 kPa) was 15 ± 1 nm and decreased to 9 ± 1 nm when the plasma gas flow rate was increased to 75 L/min (25 °C, 86.1 kPa), as shown in Fig. 6.

Effect of secondary plasma gas (H_2) addition

Experiments were conducted to evaluate the effect of adding hydrogen in the plasma flame while keeping all other conditions the same [flow rate of the primary plasma gas (Ar) of 29 L/min (25 °C, 86.1 kPa), C/W ratio of 6.3, WCl_6 feeding rate of 3.5 g/min, and flow rate of Ar–CH_4 mixture to carry the WCl_6 powder of 2.5 L/min (25 °C, 86.1 kPa) with no H_2]. The addition of secondary plasma gas (H_2) into the plasma flame plays an important role to increase the plasma flame temperature as well as to enlarge the high-temperature region [36]. The secondary plasma gas (H_2) was added at a composition of Ar-2 mol% H_2 or Ar-7 mol% H_2 in the plasma flame, which resulted in a H_2 flow rate of 0.66 L/min (25 °C, 86.1 kPa) or 2.1 L/min (25 °C, 86.1 kPa), respectively. The applied power of the plasma torch was 13 kW when no secondary plasma gas (H_2) was added and increased to about 18 kW when the secondary plasma gas (H_2) was added at 0.66 L/min (25 °C, 86.1 kPa) or 2.1 L/min (25 °C, 86.1 kPa). From the results, the predominant phase obtained under these conditions was WC_{1-x} with a small amount of WC, as shown in Fig. 7. The grain size of WC_{1-x} was 15 ± 1 nm when no secondary plasma gas (H_2) was added and increased to 18 ± 1 nm when the secondary plasma gas (H_2) was delivered at 0.66 L/min (25 °C, 86.1 kPa). However, the grain size decreased to 16 ± 1 nm when the secondary plasma gas (H_2) was increased to 2.1 L/min (25 °C, 86.1 kPa). The maximum amount of WC was observed when the secondary plasma gas (H_2) was delivered at 0.66 L/min (25 °C, 86.1 kPa). The addition of the

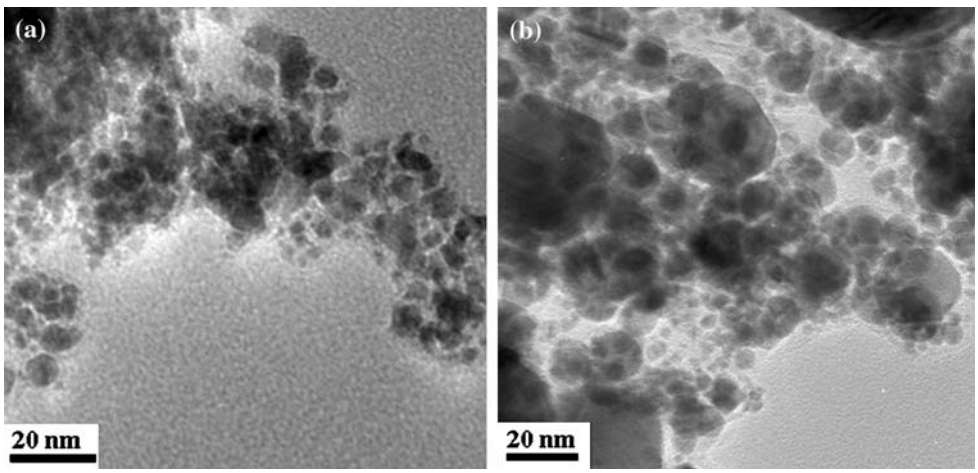

Fig. 4 TEM micrographs of WC_{1-x} nanopowder synthesized at different power levels of plasma torch: (**a**) 11 kW and (**b**) 32 kW

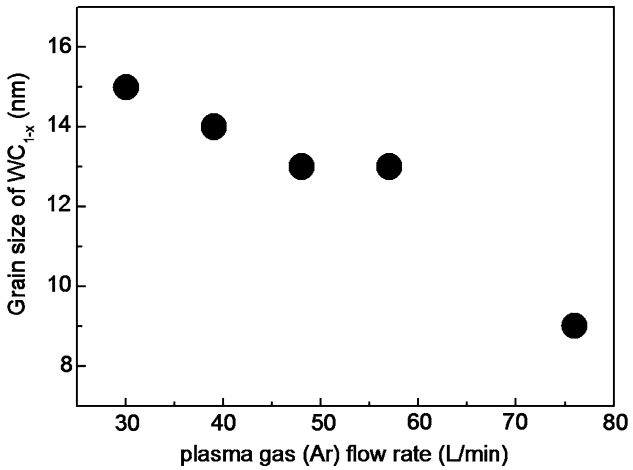

Fig. 6 Effect of plasma gas flow rate on the grain size of WC_{1-x}

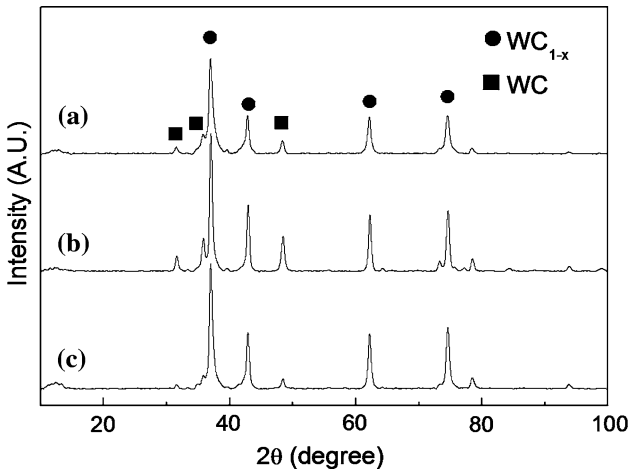

Fig. 7 X-ray diffraction patterns of the products obtained with various flow rates of the secondary plasma gas (H_2): (a) 0, (b) 0.66 L/min (25 °C, 86.1 kPa), and (c) 2.1 L/min (25 °C, 86.1 kPa)

secondary plasma gas (H_2) into the plasma flame promoted further conversion of WC_{1-x} to WC, which resulted from the increased reaction time provided by the expanded flame length. Each of the runs was repeated 2 or 3 times, and thus the variation in grain size and product composition is reproducible. However, since the differences were rather small, no further examination of the reasons for the variation was performed.

Effect of methane concentration in the feed stream

Free carbon was always present in the product since excess methane was used in the reaction. Thus, the effect of methane concentration in the feed stream was investigated by varying the C/W ratio from 6.3 to 1.5 while maintaining all other conditions constant [WCl_6 feeding rate of 3.5 g/min, flow rate of Ar–CH_4 mixture to carry the WCl_6 powder of 2.5 L/min (25 °C, 86.1 kPa) with no H_2, plasma torch power of 13 kW, and flow rate of the primary plasma gas (Ar) of 57 L/min (25 °C, 86.1 kPa) in which no secondary plasma gas (H_2) was used]. In case of the lowest C/W ratio, the ratio of H_2 produced from CH_4 to H_2 required to reduce precursor was unity. Figure 8 shows the XRD patterns of the products obtained with different C/W ratios in the feed stream. The main product obtained under these conditions was WC_{1-x} with a small amount of W_2C or WC. The formation of WC was suppressed and the presence of W_2C was observed as the methane concentration in the feed stream was decreased. The grain size of WC_{1-x} was 13 ± 1 nm at C/W ratio of 6.3 and it was not affected by decreasing the methane concentration in the feed stream within the range tested. The weight percent of carbon in the product was converted to percent (%) excess carbon, which is defined as the percentage of the excess carbon over the corresponding stoichiometric amount if all W was present as WC. The % excess carbon in the product obtained at a C/W ratio of 6.3 in the feed stream was 219%. It decreased to 26% as the C/W ratio in the feed stream was decreased to 1.5. The presence of free carbon was still observed even at the lowest C/W ratio in the feed stream. However, the free carbon also can be removed by post-treatment using hydrogen gas as discussed in the following section.

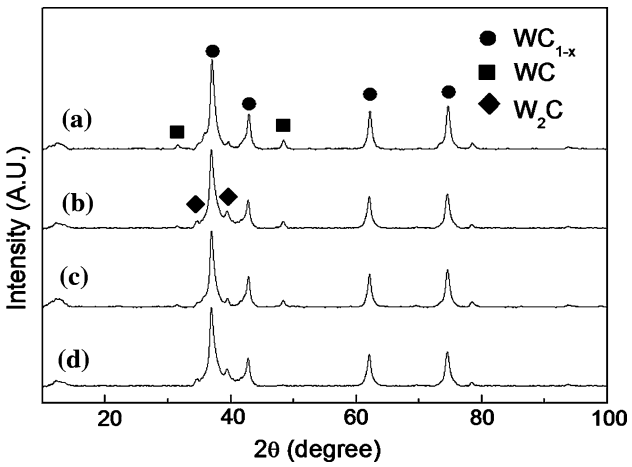

Fig. 8 X-ray diffraction patterns of the products obtained with different C/W ratios in the feed stream: (a) 6.3, (b) 4.6, (c) 2.5, and (d) 1.5

Removal of free carbon from the produced powder

As mentioned in the previous section, free carbon was always present in the produced powder since excess methane was used in the reaction. Thus, the powder obtained from the plasma reactor was placed in a ceramic boat, which in turn was placed in a tube furnace under H_2

atmosphere. The effect of hydrogen heat treatment on the product composition, grain growth, and carbon content was investigated. The amount of powder treated was 10 g, the treatment temperature was 900 °C, which was low enough to prevent rapid grain growth of particles, the ramping rate of tube furnace to increase the temperature up to 900 °C was 10 °C/min and the cooling rate to room temperature was also 10 °C/min, and hydrogen was flowed at a rate of 0.5 L/min (25 °C, 86.1 kPa) after the temperature reached 900 °C. The result showed that the unreacted WC_{1-x} and W_2C phases were fully carburized to WC phase during this post-treatment, as shown in Fig. 9. It is likely that the carburization of WC_{1-x} and W_2C phases to fully carburized WC phase occurs at this temperature by highly mobile hydrocarbon, mainly CH_4 formed during the hydrogen post-treatment, which reacts with WC_{1-x} and W_2C particles.

The excess carbon in the product, 213.5% before the treatment was completely removed after the powder was treated for 5 h, as shown in Fig. 10. The grain size of WC_{1-x} was 13 ± 1 nm before the treatment and WC powder with grain size of 36 ± 1 nm was obtained after the treatment. Figure 11 shows the TEM micrographs of WC_{1-x} powder obtained at 13 kW torch power and the WC powder obtained after the hydrogen heat treatment for 5 h. The particle size of WC_{1-x} powder was less than about 20 nm before the treatment and the particle size of WC obtained after the treatment was less than about 100 nm from measurements on a limited number of particles. As shown in the TEM micrograph, grain growth and agglomeration of particles were observed after the treatment. Since the grain growth occurred during the treatment at this temperature, the powder obtained from the plasma reactor was also treated at 800 °C. Figure 12 shows the XRD patterns of the products obtained from 2 and 5 h of hydrogen treatment at 800 °C. The main product after the treatment was W_2C with a small amount of WC, which already existed before the treatment. It can be seen that at this temperature WC_{1-x} was decarburized to the W_2C phase rather than being carburized to the WC phase, even though excess carbon was present during the hydrogen treatment. The % excess carbon, as defined in the previous section, in the product before the treatment was 213% and decreased to −39% after the powder was treated for 5 h at 800 °C. From the results, it was considered that the post-treatment temperature of powders obtained from the plasma reactor should be higher than 900 °C to produce the fully carburized WC phase.

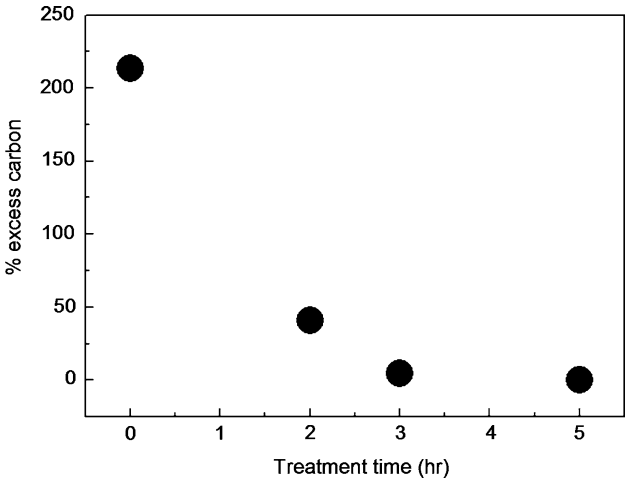

Fig. 10 Effect of hydrogen heat treatment time at 900 °C on the % excess carbon

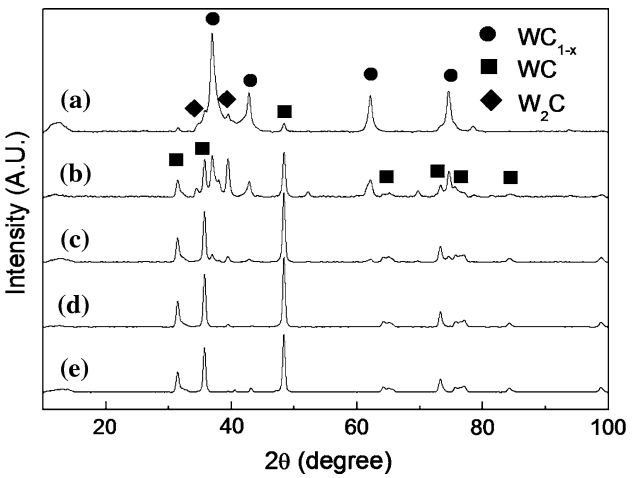

Fig. 9 X-ray diffraction patterns of the products obtained with different hydrogen treatment times at 900 °C using the powder produced from the plasma reactor: (a) before treatment, (b) 1 h, (c) 2 h, (d) 3 h, and (e) 5 h

Conclusion

Nanosized tungsten carbide powder was obtained by a thermal plasma process using tungsten hexachloride (WCl_6) as the precursor. The experimental results showed that nanosized WC_{1-x} powder, which sometimes contained small amounts of WC and/or W_2C phase, can be synthesized using WCl_6 and CH_4 as the starting materials by the thermal plasma process. The amounts of WC and W_2C in the product decreased with an increase in the plasma torch power and the plasma gas flow rate. The particle size of WC_{1-x} was affected by plasma torch power, the plasma gas flow rate, and the addition of secondary plasma gas (H_2), but not by the methane concentration within the range tested. The produced WC_{1-x} and W_2C phases were carburized to the fully carburized WC phase and excess carbon in the product was completely removed by the hydrogen post-treatment at 900 °C. The particle size of

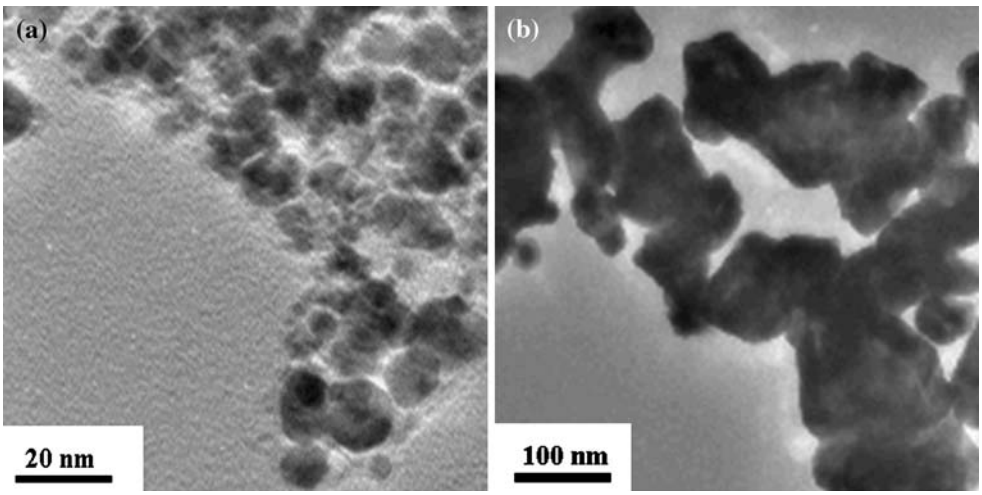

Fig. 11 TEM micrographs of powders: (**a**) WC_{1-x} powder obtained from the plasma reactor and (**b**) WC powder obtained after the hydrogen treatment for 5 h at 900 °C

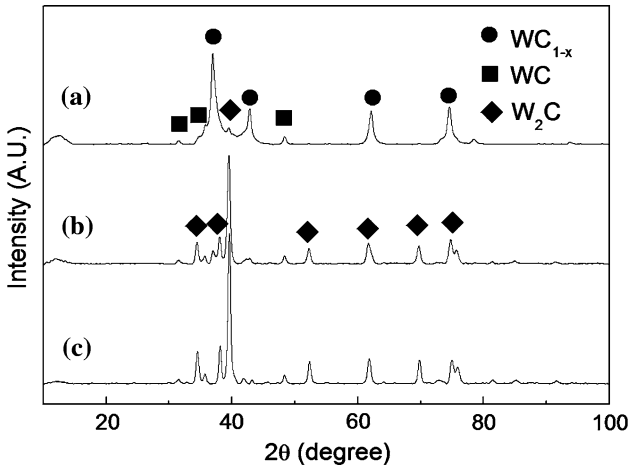

Fig. 12 X-ray diffraction patterns of the products obtained with different hydrogen heat treatment times at 800 °C using the powder obtained from the plasma reactor: (a) before treatment, (b) 2 h, and (c) 5 h

WC_{1-x} obtained by the thermal plasma process was less than about 20 nm and WC powder having particle size less than 100 nm with grain size less than 40 nm was obtained after the hydrogen post-treatment of the produced WC_{1-x} powder. The CVS conducted in a thermal plasma system has confirmed its feasibility for the preparation of nano-sized powders. This process is also suitable for large-scale production of nanosized tungsten carbide powders since the plasma process can work continuously.

Acknowledgements This material is based upon the work supported by the US Department of Energy under Award No. DE-FC36-04GO14041 with cost sharing by Kennametal and Smith International and technical collaboration with Idaho National Laboratory. The authors wish to thank Prof. Patrick R. Taylor of Colorado School of Mines for his help with the selection, design, and initial operation of the plasma reactor system. Thanks also go to Mr. Robert W. Byrnes of the University of Utah for his competent work with the design and repair of the experimental facilities.

References

1. Upadhaya GS (2002) Cemented tungsten carbide. Noyes Publications, New York
2. Petersson A, Ågren J (2004) Acta Mater 52:1847. doi:10.1016/j.actamat.2003.12.024
3. Fang Z, Maheshwari P, Wang X et al (2005) Inter J Refract Metab Hard Mater 23:249. doi:10.1016/j.ijrmhm.2005.04.014
4. Lee G-H, Kang S (2006) J Alloy Comp 419:281. doi:10.1016/j.jallcom.2005.09.060
5. Wahlberg S, Grenthe I, Muhammed M (1997) Nanostruct Mater 9:105. doi:10.1016/S0965-9773(97)00029-9
6. Zhu YT, Manthiram A (1996) Compos Part B Eng 27:407
7. Fu L, Cao LH, Fan YS (2001) Scr Mater 44:1061. doi:10.1016/S1359-6462(01)00668-6
8. Nersisyan HH, Won HI, Won CW et al (2005) Mater Chem Phys 94:153. doi:10.1016/j.matchemphys.2005.04.024
9. Wu XY, Zhang W, Wang W et al (2004) J Mater Res 19:2240. doi:10.1557/JMR.2004.0324
10. Zawrah MF (2007) Ceram Int 33:155. doi:10.1016/j.ceramint.2005.09.010
11. Shi XL, Shao GQ, Duan XL et al (2006) Mater Charact 57:358. doi:10.1016/j.matchar.2006.02.013
12. McCandlish LE, Kear BH, Kim BK (1992) Nanostruct Mater 1:119. doi:10.1016/0965-9773(92)90063-4
13. Ban Z-G, Shaw LL (2002) J Mater Sci 37:3397. doi:10.1023/A:1016553426227
14. Hasanpour A, Mozaffari M, Amighian J (2007) Physica B (Amsterdam) 387:298. doi:10.1016/j.physb.2006.04.039
15. Liu S, Huang Z-L, Liu G et al (2006) Inter J Refract Metab Hard Mater 24:461. doi:10.1016/j.ijrmhm.2005.10.001
16. Mi S, Courtney TH (1997) Scr Mater 38:171. doi:10.1016/S1359-6462(97)00410-7
17. Chang W, Skandan G, Hahn H et al (1994) Nanostruct Mater 4:345. doi:10.1016/0965-9773(94)90144-9
18. Tong L, Reddy RG (2005) Scr Mater 52:1253. doi:10.1016/j.scriptamat.2005.02.033

19. Moriysohi Y, Futaki M, Komatsu S et al (1997) J Mater Sci Lett 16:347. doi:10.1023/A:1018586009506
20. Fukumasa O, Fujiwara T (2003) Thin Solid Films 435:33. doi:10.1016/S0040-6090(03)00371-7
21. Swihart MT (2003) Curr Opin Colloid In 8:127. doi:10.1016/S1359-0294(03)00007-4
22. Gao Y, Guo X-P, Wei R (2006) Surf Coat Tech 201:2829. doi:10.1016/j.surfcoat.2006.05.035
23. Tong L, Reddy RG (2006) Mater Res Bull 41:2303. doi:10.1016/j.materresbull.2006.04.021
24. Mohai I, Gál L, Szépvölgyi J et al (2007) J Eur Ceram Soc 27:941. doi:10.1016/j.jeurceramsoc.2006.04.128
25. Hojo J, Oku T, Kato A (1978) J Less Common Met 59:85. doi:10.1016/0022-5088(78)90114-5
26. Fitzsimmons M, Sarin VK (1995) Surf Coat Tech 76:250
27. Kim JC, Kim BK (2004) Scr Mater 50:969. doi:10.1016/j.scriptamat.2004.01.015
28. Tang X, Haubner R, Lux B et al (1995) J Phys II 5:1013. doi:10.1051/jp3:1995174
29. Won C-W, Chun B-S, Sohn HY (1993) J Mater Res 8:2702. doi:10.1557/JMR.1993.2702
30. Leclercq G, Kamal M, Giraudon JM et al (1996) J Catal 158:142. doi:10.1006/jcat.1996.0015
31. Kelly CM, Garg D, Dyer PN (1992) Thin Solid Films 219:103. doi:10.1016/0040-6090(92)90729-U
32. Medeiros FFP, Oliveira SAD, Souza CPD et al (2001) Mater Sci Eng A 315:58. doi:10.1016/S0921-5093(01)01214-X
33. Gao L, Kear BH (1995) Nanostruct Mater 5:555. doi:10.1016/0965-9773(95)00265-G
34. Cullity BD (1978) Elements of X-ray diffraction, 2nd edn. Addison-Wesley Pub. Co, London
35. Sara RW (1965) J Am Ceram Soc 48:253
36. Choi SI, Nam JS, Lee CM et al (2006) Curr Appl Phys 6:224. doi:10.1016/j.cap.2005.07.045